Progress In Electromagnetics Research C, Vol. 173, 321–330, 2026

PIER C

(Received 9 August 2026, Accepted 9 September 2026, Scheduled 21 September 2026)

A Concentric Multi-Ring Circular Monopole Antenna Designed by Characteristic Mode Analysis for Continuous Sub-6 GHz 5G Coverage

Immanuel P. Soundararajan[1,*], Muthurajan Subramoniam[2], Arul Kulandaivel[3], Lakshmi Dhandapani[1], and Rajesh K. Dhandapani[4]

[1]*Department of Electrical and Electronics Engineering*
Academy of Maritime Education and Training (AMET) Deemed to be University, Chennai, Tamil Nadu 603112, India
[2]*Department of Marine Engineering*
Academy of Maritime Education and Training (AMET) Deemed to be University, Chennai, Tamil Nadu 603112, India
[3]*Department of Robotics and Automation Engineering*
Dhaanish Ahmed Institute of Technology, Coimbatore, Tamil Nadu 641105, India
[4]*Department of Electronics and Communication Engineering*
Vel Tech Rangarajan Dr. Sagunthala R&D Institute of Science and Technology, Chennai, Tamil Nadu 600062, India

ABSTRACT: This paper presents a single-port concentric multi-ring circular monopole in which each ring is a separate characteristic-mode resonator, and cross spokes force the ring currents in phase so that the individual ring resonances merge into one continuous impedance band. This ring-per-mode partitioning distinguishes the design from single-mode monopoles, and characteristic mode analysis (CMA) is used to place and order the modes rather than explain a finished geometry. The radiator occupies $0.27\lambda_0 \times 0.39\lambda_0$ on a $33 \times 23 \times 0.8\,\mathrm{mm}^3$ RT/Duroid 5880 substrate ($\varepsilon_r = 2.2$, $\tan\delta = 0.0009$), a low-permittivity laminate that resists miniaturisation. A central disc of radius 5.5 mm and three concentric rings of mean radii 6.27, 7.79, and 10.14 mm are excited by a 50 Ω microstrip line whose 2.465 mm width follows directly from Hammerstad synthesis, and a triangular tapered partial ground of height 10.66 mm — one quarter-wavelength at band centre completes the match. Closed-form ring resonances of 3.72, 4.84 and 6.02 GHz agree with the modal spectrum and with the measured lower resonance at 3.65 GHz to within 1.9%. The measured impedance band spans 3.50–6.15 GHz, a fractional bandwidth of 54.9% centered at 4.83 GHz, and covers the 5G NR n77, n78 and n79 bands together with the 5.5 GHz WLAN band in one continuous match. A physically partitioned equivalent circuit, one series-RLC branch per ring with every branch resonance fixed to its closed-form value, reproduces the full-wave reflection response with a 0.72 dB RMS error. The design gives a compact, single-layer, single-feed route to full sub-6 GHz coverage with an analysis chain that ties every dimension to a resonant mechanism.

1. INTRODUCTION

Sub-6 GHz 5G New Radio places the n77 (3.30–4.20 GHz), n78 (3.30–3.80 GHz), and n79 (4.40–5.00 GHz) bands close together, and a single terminal antenna that covers all three in one continuous match removes the need for band switching. A printed monopole is the natural candidate because it is planar, low-profile, and easy to integrate, but a plain monopole radiates on one dominant mode, and its impedance band is narrow. Widening that band without adding layers or lumped tuning is the design problem this paper addresses.

Multiple resonators sharing one feed is a standard route to a wide band, but yet trial reshaping usually introduces resonators. Their interaction is read afterward from surface currents. Characteristic mode analysis inverts that order. Characteristic mode theory computes a conductor's resonant current modes before any feed is placed [1, 2], and equivalent-circuit descriptions built on those modes connect the modal spectrum to a lumped impedance [3]. Used as a design tool rather than a diagnostic, CMA lets the geometry be shaped so that several modes resonate in a chosen band and radiate compatibly, which is exactly what a wideband monopole needs.

This paper applies that idea to a concentric ring geometry. A central disc and three concentric rings, tied together by cross spokes, present a set of ring modes whose resonant frequencies are set by the ring radii. The spokes hold the ring currents in phase so the ring resonances overlap instead of interfere, and a triangular tapered partial ground converts the overlapped resonances into a single matched band. Every ring maps to one resonance; every resonance maps to one closed-form frequency; and the same partition carries through to the equivalent circuit.

The contributions are as follows.

- A concentric multi-ring monopole in which each ring is an independent characteristic-mode resonator, and cross spokes merge ring resonances into one continuous 54.9% band from a single port.
- A CMA-driven design flow that places and orders the ring modes before feeding, supported by closed-form ring-

* Corresponding author: Immanuel Prabaharan Soundararajan (imman.amet@gmail.com).

resonance equations that predict band edges to within 1.9% of measurement.

- A triangular tapered partial ground, one quarter-wavelength at band centre, which completes the wideband match, with a parametric study isolating its effect.
- A physically partitioned equivalent circuit — one series-RLC branch per ring, each branch resonance fixed to its closed-form value that reproduces the full-wave reflection response to 0.72 dB root-mean-square (RMS) while keeping every element interpretable.

Novelty and contributions. The novelty of this work is a concentric multi-ring monopole in which each ring is treated as an independent characteristic-mode resonator, and the contribution is the complete analytical chain that this partitioning enables. Unlike single-ring or disc monopoles, whose wide band comes from one empirically broadened resonance, three concentric rings of distinct mean radii here resonate at distinct closed-form frequencies (3.72, 4.84, and 6.02 GHz), and cross spokes hold the ring currents in phase so the separate resonances merge into one continuous 54.9% band from a single feed. Three elements, not previously reported together, follow: (i) CMA is used as a forward design tool that places and orders the ring modes before the feed is applied, rather than as an after-the-fact diagnostic; (ii) closed-form ring-resonance equations predict the measured band edges to within 1.9%, tying every physical dimension to a resonant mechanism; and (iii) a physically partitioned equivalent circuit — one series-RLC branch per ring, each branch resonance fixed to its closed-form value rather than fitted — reproduces the full-wave reflection response to 0.72 dB RMS while keeping every element interpretable. The design further shows that continuous sub-6 GHz coverage is achievable on a low-permittivity RT/Duroid 5880 laminate within $0.27\lambda_0 \times 0.39\lambda_0$, whereas most compact sub-6 designs rely on high-permittivity FR-4 to assist miniaturisation.

2. RELATED WORK AND RESEARCH GAP

2.1. Ring and Disc Monopoles for Sub-6 GHz

Circular-ring monopoles give wide impedance bands with a compact footprint. A circular ring monopole with a multiple-input multiple-output (MIMO) extension covered a sub-6/sub-7 GHz band from 3.2 to 7.3 GHz alongside a millimetre-wave band [4]. A clock-shaped radiator built from a circular ring and two crossed microstrip lines produced broadband circular polarisation, with CMA used to explain the orthogonal modes [5]. An eight-element array of dual-arm tortuous monopoles with ground stubs covered 3.2–6.0 GHz across three resonances for 5G smartphones [15]. These works confirm that ring and multi-branch monopoles reach wide bands, but the resonators are shaped empirically rather than assigned mode by mode.

Two closely related single-ring realisations further frame the present contribution. An early printed circular ring monopole obtained a wide match from a single continuous ring by empirically tuning the inner and outer radii, without modal assignment or a closed-form model [17]. More recently, a comparable outline was implemented in conductive fabric on a textile substrate for on-body internet of things (IoT) use, where the contribution lies in the flexible-material realisation rather than in a modal design method [18]. In contrast, the proposed radiator uses several concentric rings of distinct radii, each an independent characteristic-mode resonator whose frequency is fixed in closed form, so the wide band is assembled mode by mode rather than obtained from a single continuous ring.

2.2. Characteristic Mode Analysis in Antenna Design

CMA has moved from a diagnostic into a design method. A systematic procedure used CMA to design a broadband circularly polarised slot monopole before excitation [6]. A crescent-moon monopole with ground modifications used CMA to generate orthogonal modes and reach a 61.2% impedance band [7]. A quad-element sub-6 GHz MIMO array used CMA to raise gain and isolation [8]. A multiband patch superimposed lower- and higher-order modes at a common frequency to enhance broadside radiation [9], and orthogonal modes on a single substrate were excited for a wideband millimetre-wave design [10]. Across these works, CMA typically targets one or two modes for a single band or for polarisation; systematic use of many ring modes to fill one continuous sub-6 band is uncommon.

2.3. Multi-Element and Slot Approaches

Slot and multi-element structures reach the same bands by other means. A dual-band elliptical-ring-slot MIMO antenna produced orthogonal circular polarisation across 3.55–3.80 and 4.60–4.80 GHz [11]. Orthogonally placed microstrip monopoles with inverted-L slots gave dual- and triple-band operation for n77/n78/n79 [12]. A quad-port U-slot monopole MIMO covered the n77/n78 bands with a rotational-symmetry decoupler [13]. An octagonal MIMO system reached broadband operation with enhanced isolation [14]. These designs meet the bands but through multiple narrow resonances or multiple ports rather than one continuous single-port match, and most are built on FR-4.

Multi-antenna terminals additionally require that closely spaced elements be decoupled, and a substantial literature addresses this. Bait-Suwailam et al. demonstrated metamaterial-inspired decoupling and etched slotted complementary split-ring resonators between microstrip patches to suppress mutual coupling through a localized negative-permeability response [19]. At the system level, a dual-polarized eight-port diversity MIMO array for 5G smart terminals covered 3.38–3.80 GHz using octagonal ground-plane slots, with an envelope correlation coefficient below 0.055 and diversity gain above 9.95 [20]. A highly self-isolated twelve-element array at 3.42–3.62 GHz reached isolation better than -19 dB and an ECC below 0.006 through orthogonal element placement [21]. These works establish the decoupling and diversity techniques on which a multi-element deployment would rely; the present paper contributes single radiating element — a compact, continuously matched, analytically designed sub-6 monopole — that such techniques would replicate and isolate.

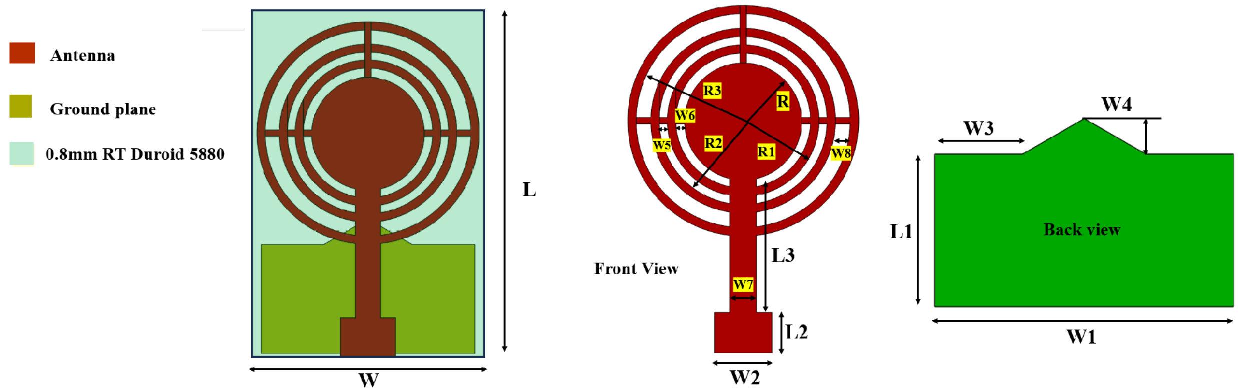

FIGURE 1. Overall structure and dimensions of the proposed antenna.

2.4. Research Gap

Three gaps follow from the survey. First, ring and disc monopoles are widened by empirical reshaping, so the contribution of each ring to the band is not established before feeding. Second, CMA is used mostly to secure one or two modes for a single band, not to orchestrate a set of concentric-ring modes into one continuous wide band. Third, most compact sub-6 designs use high-permittivity FR-4, where a high dielectric constant assists miniaturisation, whereas low-permittivity laminates, such as RT/Duroid 5880, are harder to shrink and seldom used for a fully continuous sub-6 monopole.

The proposed antenna addresses each gap. Each concentric ring is treated as a distinct characteristic-mode resonator whose frequency is fixed by its radius, so the band is assembled mode by mode. CMA places and orders those modes before addomg the feed, and cross spokes merge them into one 54.9% band. The whole radiator sits on RT/Duroid 5880 within $0.27\lambda_0 \times 0.39\lambda_0$, showing that continuous sub-6 coverage is reachable on a low-permittivity substrate.

3. ANTENNA GEOMETRY AND CLOSED-FORM DESIGN

Figure 1 shows the geometry. The radiator is a central solid disc of radius $R = 5.5$ mm surrounded by three concentric annular rings of mean radii $R1 = 6.27$ mm, $R2 = 7.79$ mm, and $R3 = 10.14$ mm, connected to the disc and to one another by cross spokes. A $50\,\Omega$ microstrip line of width $W7 = 2.465$ mm and length $L3 = 12.62$ mm feeds the radiator through a short low-impedance matching pad of width $W2 = 5.423$ mm. The back face carries a triangular tapered partial ground of width $W1 = 20.938$ mm and height $L1 = 10.66$ mm. The board is $33 \times 23 \times 0.8\,\text{mm}^3$ RT/Duroid 5880 with $\varepsilon_r = 2.2$ and $\tan\delta = 0.0009$. Table 1 lists all dimensions.

The feed width sets the reference impedance. For a microstrip line of width W on a substrate of height h and permittivity ε_r, the effective permittivity and characteristic impedance follow the Hammerstad forms,

$$\varepsilon_{\mathit{eff}} = \frac{\varepsilon_r + 1}{2} + \frac{\varepsilon_r - 1}{2}\left(1 + \frac{12h}{W}\right)^{-1/2} \tag{1}$$

TABLE 1. Various design parameters of the proposed antenna.

Par.	Value (mm)	Par.	Value (mm)	Par.	Value (mm)
L	33	$W2$	5.423	$W8$	1.3752
$L1$	10.66	$W3$	6.1352	R	5.5
$L2$	3.8	$W4$	4.3767	$R1$	6.27
$L3$	12.62	$W5$	0.7582	$R2$	7.79
W	23	$W6$	0.8233	$R3$	10.14
$W1$	20.938	$W7$	2.465		

$$Z_0 = \frac{120\pi}{\sqrt{\varepsilon_{\mathit{eff}}}\left[\frac{W}{h} + 1.393 + 0.667\ln\left(\frac{W}{h} + 1.444\right)\right]} \tag{2}$$

With $W = 2.465$ mm and $h = 0.8$ mm, the ratio $W/h = 3.081$ gives $\varepsilon_{\mathit{eff}} = 1.871$ and $Z_0 = 50.28\,\Omega$, so the feed width in Table 1 is the synthesised $50\,\Omega$ width rather than a tuned value.

Each ring resonates when its mean circumference is near one guided wavelength. Treating a ring of mean radius r as an ungrounded printed loop with $\varepsilon_{\mathit{eff}} = (\varepsilon_r + 1)/2$, the ring resonance is

$$f_{\text{ring}} = \frac{c}{2\pi r\sqrt{(\varepsilon_r + 1)/2}} \tag{3}$$

Equation (3) gives 3.72 GHz for the outer ring, 4.84 GHz for the middle ring, 6.02 GHz for the inner ring, and 6.86 GHz for the disc. The outer ring sets the lower band edge, and its 3.72 GHz prediction matches the measured lower resonance at 3.65 GHz to within 1.9%. The inner rings and disc supply the upper resonances, an ordering confirmed by the surface currents of Section 7.

The partial ground acts as the counterpoise. Its height $L1 = 10.66$ mm equals one quarter guided wavelength at the 4.83 GHz band centre, where (1) with the ground width gives $\lambda_g/4 = 10.72$ mm. The tapered top edge grades the ground-to-radiator transition and widens the match, as shown in Section 6. The matching pad of width $W2 = 5.423$ mm presents $Z_0 = 28.1\,\Omega$ from (2), a short low-impedance transformer between the $50\,\Omega$ line and the radiator node.

The radiator is electrically small. At the 3.50 GHz lower edge, the free-space wavelength is 85.7 mm, so the board

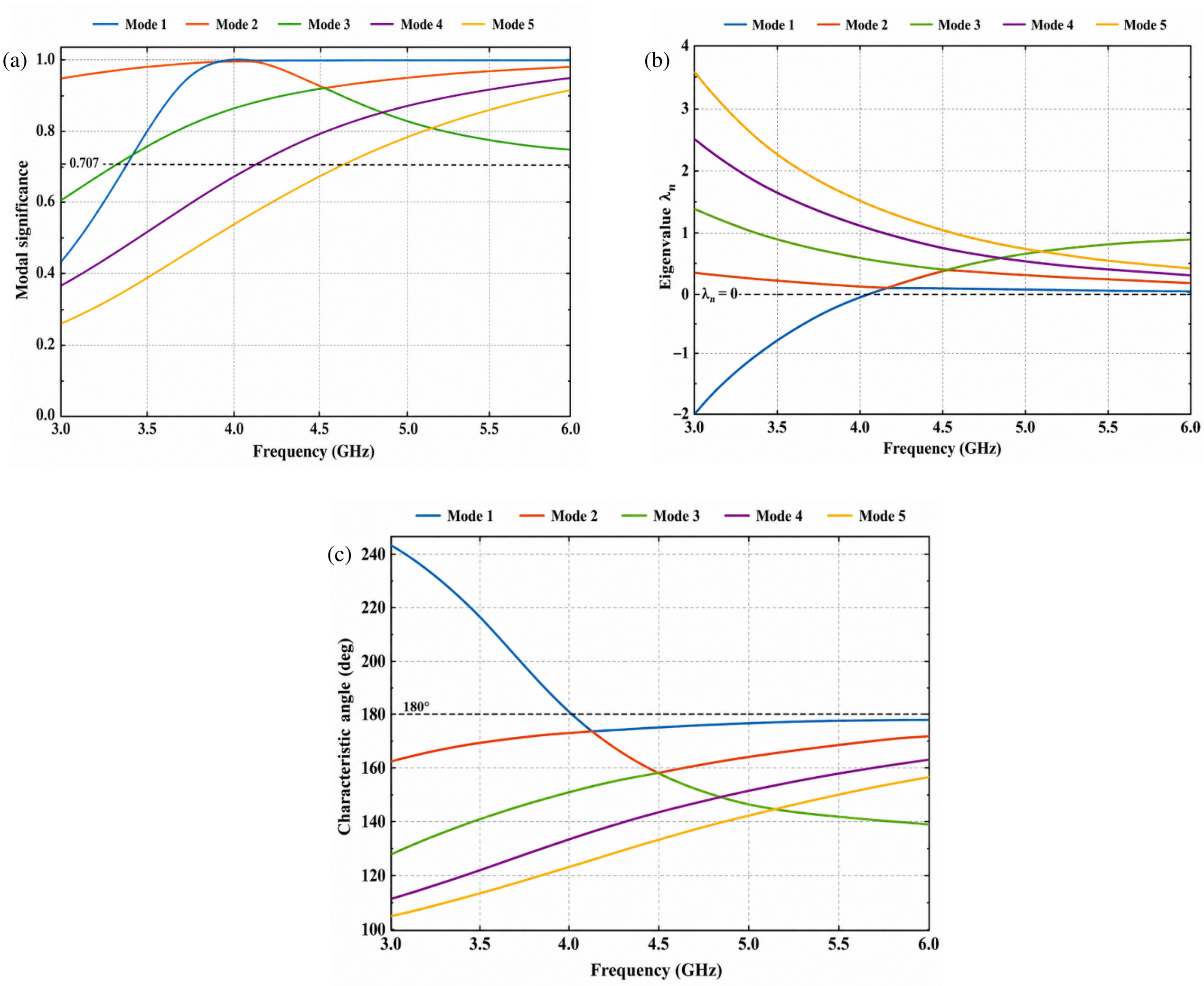

FIGURE 2. Characteristic mode analysis at 4 GHz.

measures $0.269\lambda_0 \times 0.385\lambda_0$, and the outer ring diameter is $0.237\lambda_0$.

4. CHARACTERISTIC MODE ANALYSIS

Ring modes are examined with CMA before applying the feed. Fig. 2 shows the modal significance, eigenvalues λ_n, and characteristic angles of the low-order modes across the band. A mode radiates efficiently where its modal significance approaches unity, equivalently where its eigenvalue crosses zero, and its characteristic angle passes 180°,

$$\mathrm{MS}_n = \frac{1}{|1 + j\lambda_n|}, \quad \alpha_n = 180^\circ - \tan^{-1}(\lambda_n) \qquad (4)$$

The first mode reaches unity modal significance near 4.0 GHz, where its eigenvalue crosses zero, and its characteristic angle passes 180°. A second mode holds a modal significance above 0.9 across almost the whole band, giving the broadband backbone of the response, while higher modes become significant in the upper band and cross the 0.707 level near 3.25, 4.1 and 4.55 GHz. Several modes are therefore significant at once, which is the condition for a continuous wide band rather than a set of separated resonances.

Figure 3 shows the modal current distributions. The first mode carries current over the whole structure and the ground, the second concentrates on the central disc, and the third loads the outer ring — so the modes map onto physical parts of the radiator, and each ring can be associated with a resonance. Fig. 4 shows the corresponding three-dimensional modal patterns, each of monopole-like form with a broadside maximum, confirming that the modes radiate compatibly and combine without pattern break-up.

5. PROTOTYPE AND REFLECTION COEFFICIENT

The antenna was fabricated on RT/Duroid 5880 and fed by an SMA connector. Fig. 5 shows the prototype, with the concentric rings and cross spokes etched on the front face.

Simulation setup. All full-wave results in this work were computed in Ansys High Frequency Structure Simulator (HFSS) using its finite-element frequency-domain solver with adaptive mesh refinement and a radiation (air) boundary placed one quarter-wavelength from the radiator on all sides. The

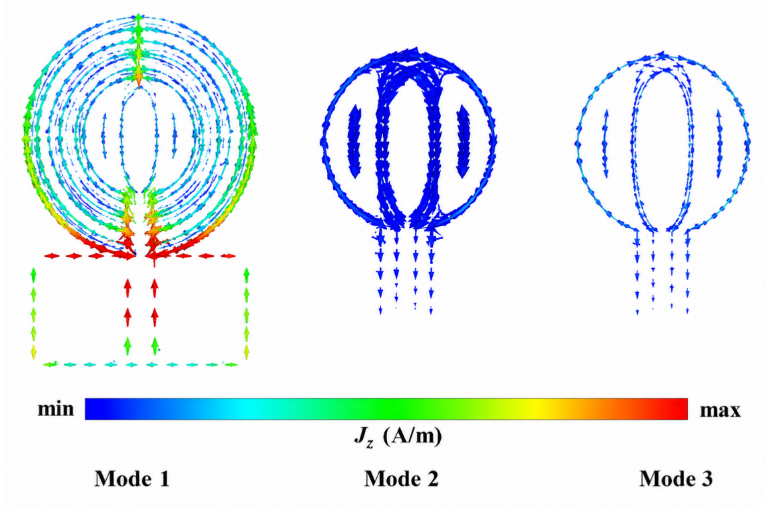

FIGURE 3. Surface current distribution for different modes.

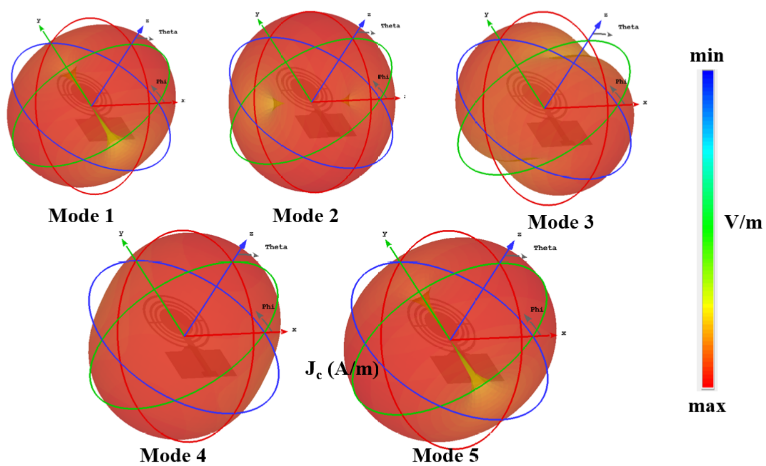

FIGURE 4. Surface current distribution for different modes.

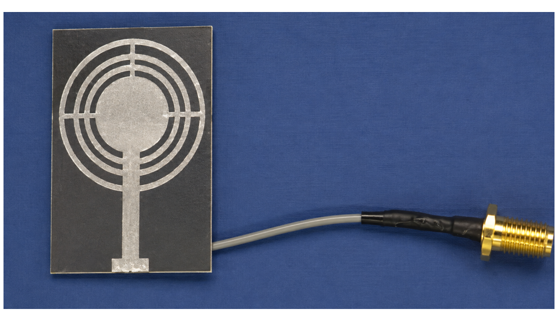

FIGURE 5. Fabricated prototype of the proposed antenna.

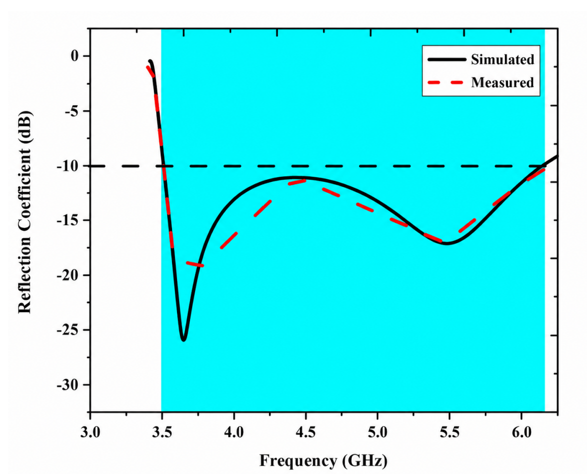

FIGURE 6. Simulated and measured reflection coefficients of the proposed antenna.

antenna was excited by a 50 Ω wave port at the microstrip feed edge, and the adaptive solution was converged to a maximum change in S-parameters below 0.02 between successive passes. The characteristic-mode data in Fig. 2 were obtained from the same HFSS model using its characteristic-mode solver on the unfed conductor, and the equivalent-circuit reflection response in Section 8 was evaluated from the extracted element values in Table 2.

Figure 6 shows simulated and measured reflection coefficients. The measured impedance band, taken at the −10 dB level, spans 3.50–6.15 GHz, a fractional bandwidth of 54.9% about a 4.83 GHz centre and a band ratio of 1.76. Two reso-

TABLE 2. Extracted equivalent-circuit element values.

Branch (ring)	f_{cf} (GHz)	f_{fit} (GHz)	R (Ω)	L (nH)	C (pF)	Q
Outer ring	3.72	3.66	71.2	13.06	0.145	4.2
Middle ring	4.84	4.87	145.1	9.80	0.109	2.1
Inner ring + disc	6.02	6.10	70.0	7.83	0.087	4.3
Feed line	—	—	$Z_0 = 50.3\,\Omega$	$\varepsilon_{eff} = 1.87$	$\ell = 12.62$ mm	—
Neck L_N	—	—	—	0.32	—	—
Gap C_g	—	—	—	—	0.15	—

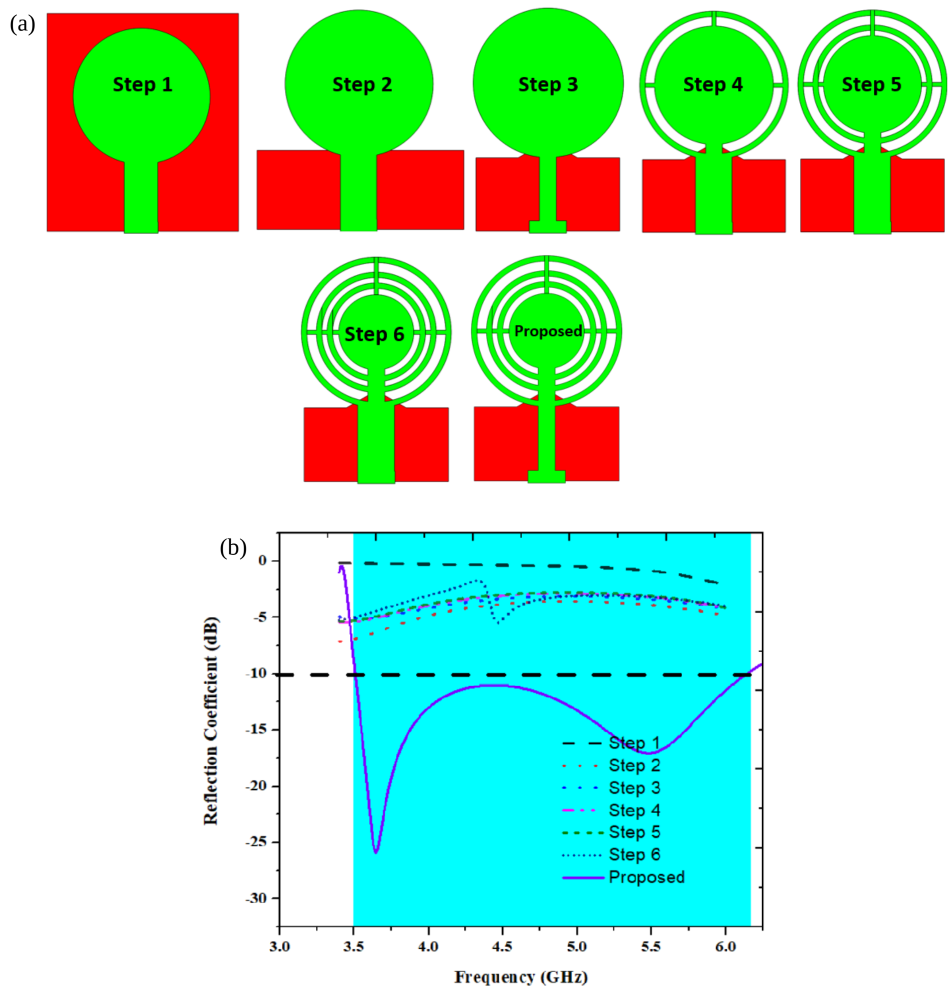

FIGURE 7. (a) Design evolution of the proposed antenna and (b) its reflection coefficient.

nances are visible: a deep one at 3.65 GHz reaching −25.8 dB and a second at 5.5 GHz reaching −17.1 dB, with the response staying below −10 dB across the mid-band dip near 4.45 GHz, so the band remains continuous. The measured and simulated curves track closely across the whole range. The band covers the n77, n78, and n79 5G NR allocations together with the 5.5 GHz WLAN band.

6. DESIGN EVOLUTION AND PARAMETRIC STUDY

Figure 7 traces the design evolution and its effect on the reflection coefficient. The steps add the disc, the successive rings, and finally the tapered ground. The early steps, with fewer rings and an untapered ground, hold the response above −10 dB across much of the band, and only the full structure with three rings and the tapered partial ground produces the continuous sub-−10 dB band — so the tapered ground is what closes the match once the ring set is in place.

Figure 8 shows the sensitivity to the two dominant dimensions. Varying the ground height $L1$ in Fig. 8(a) changes the upper band strongly: too short a ground weakens the upper resonance, and $L1 = 10.66$ mm restores it and gives the widest band — the trade is that a longer ground raises the lower edge. Varying the pad-related length $L2$ in Fig. 8(b) tunes the upper resonance and the flatness of the mid-band, with $L2 = 3.8$ mm balancing depth against bandwidth. The two dimensions act on

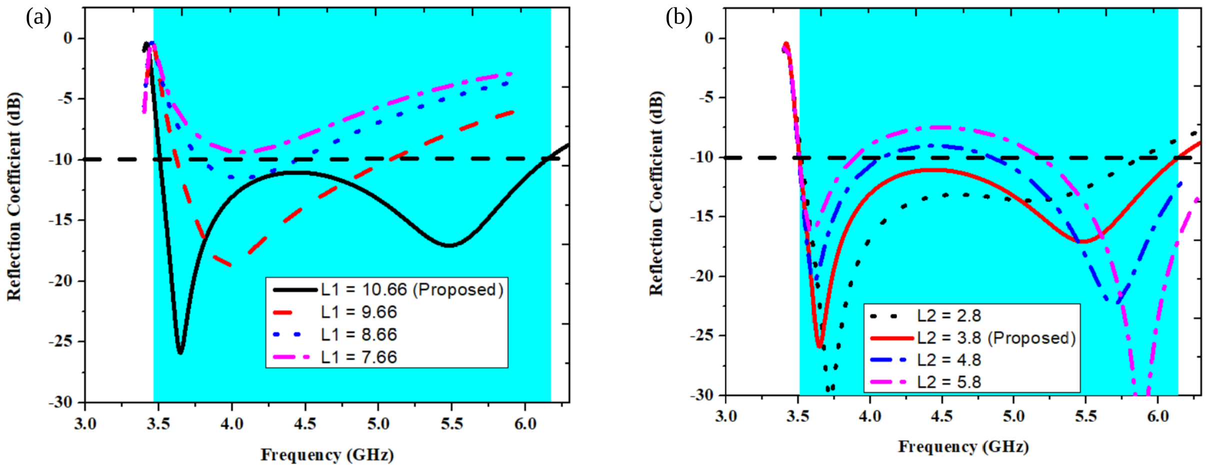

FIGURE 8. Parametric study of the proposed antenna when altering (a) $L1$ and (b) $L2$.

different parts of the band, which let the lower and upper edges be set almost independently.

7. RADIATION CHARACTERISTICS

Figure 9 shows the surface current at 3.6, 4.5, and 5.5 GHz. At 3.6 GHz, the current concentrates on the outer ring; at 4.5 GHz, it moves to the middle ring; and at 5.5 GHz, it loads the inner rings and the disc. The progression matches the closed-form ordering in (3), and the largest ring sets the lowest resonance and the inner elements the higher ones, and confirms that the band is built from distinct ring resonances rather than one distributed mode.

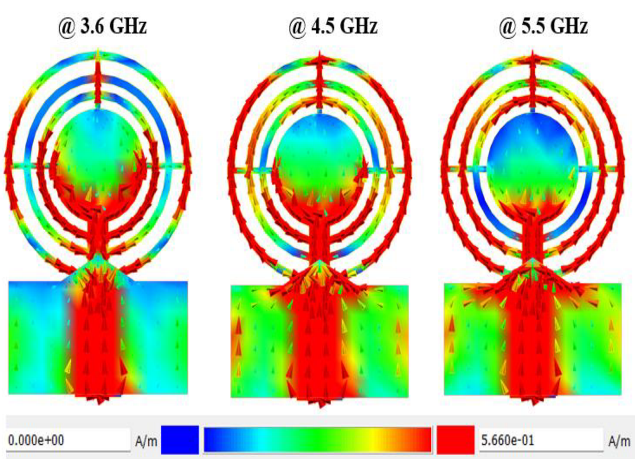

FIGURE 9. Surface current distribution of the proposed antenna at various operating frequencies.

Figure 10 shows far-field patterns at the same three frequencies. Each pattern is monopole-like, with a broadside maximum and near-omnidirectional coverage in the orthogonal plane, and the shape holds across the band. The stable pattern shows that the ring modes radiate compatibly, so combining them to widen the impedance band does not distort the radiation.

Fig. 11 shows the frequency behaviour of the realized gain and radiation efficiency. Across the operating band, the simulated realized gain rises smoothly from about 1.8 dBi near the lower edge to 4.7 dBi at 6.0 GHz, the increase following the radiator's growing electrical size with frequency, while the radiation efficiency stays high and flat between 88.6% and 91.5%, consistent with the low-loss RT/Duroid 5880 laminate ($\tan\delta = 0.0009$). The measured gain and efficiency track the simulation closely across the whole band, and the small measured shortfall (peak gain about 4.6 dBi and efficiency above 86%) is attributable to connector and cable losses and fabrication tolerance. The stable, high efficiency and the monotonic gain confirm that co-phasing ring modes to widen the impedance band does not degrade radiation.

8. EQUIVALENT CIRCUIT MODEL

An equivalent circuit ties the reflection response back to ring resonances. The model is partitioned by physical feature: each concentric ring is one series-RLC branch, and the fixed sections that can be computed outright are computed, not fitted. Building the circuit on the modal picture follows the characteristic-mode equivalent-circuit approach [3], and the series-RLC-per-resonator form follows parallel-branch monopole models used for wideband radiators [16].

Figure 12 shows the topology. The 50 Ω feed line enters as a transmission-line section of characteristic impedance 50.3 Ω, effective permittivity 1.87, and length 12.62 mm, all from (1) and (2). A short neck inductance $L\_N = 0.32$ nH, computed from the strip length and width, joins the feed to the radiator node. A shunt capacitance C_g models the gap between the feed edge and the ground plane. The three ring branches hang from the radiator node in parallel. The central disc and the innermost ring resonate together in the upper band, as the currents shown in Fig. 9, so they are represented by the single upper branch rather than by a separate disc resonator.

Each branch is a series resonator whose resonant frequency is fixed to the closed-form ring value of (3),

$$f_{0i} = \frac{1}{2\pi\sqrt{L_i C_i}}, \quad Q_i = \frac{2\pi f_{0i} L_i}{R_i} \tag{5}$$

Branch resonances are held at closed-form frequencies; the slope impedance $\sqrt{L_i/C_i}$ is fixed at 300 Ω for the ring set; and

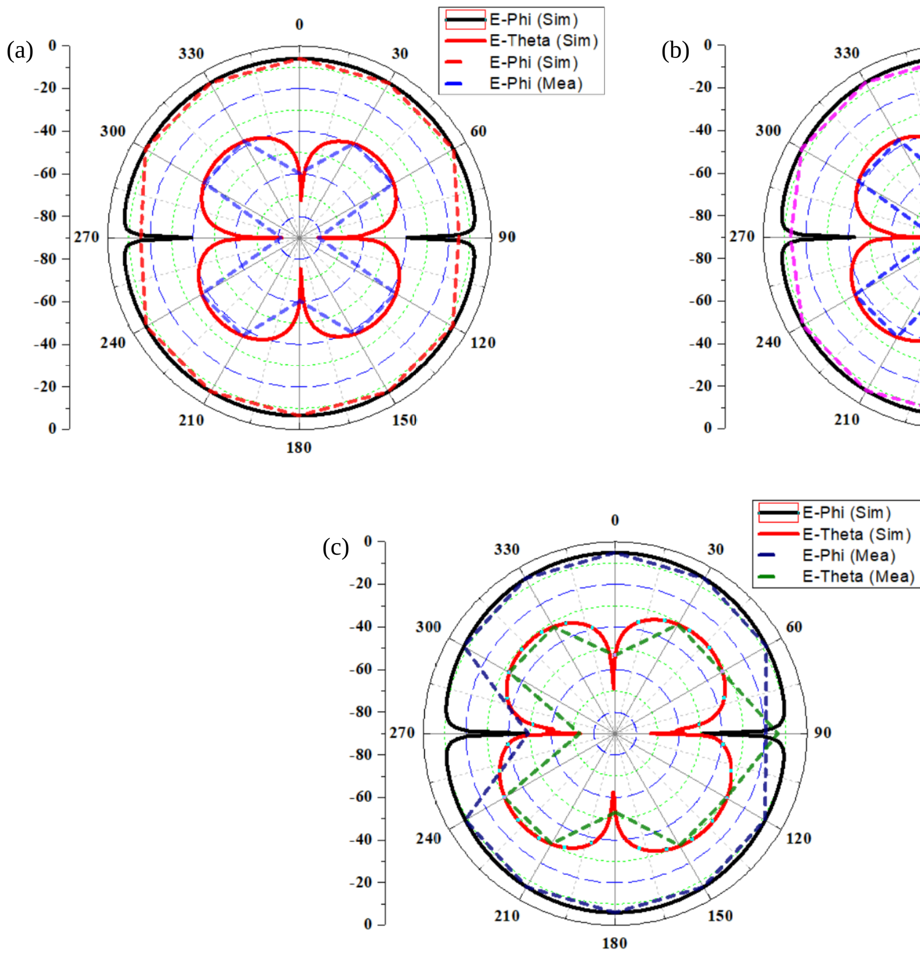

FIGURE 10. Far-field pattern of the proposed antenna at (a) 3.6 GHz, (b) 4.5 GHz, and (c) 5.5 GHz.

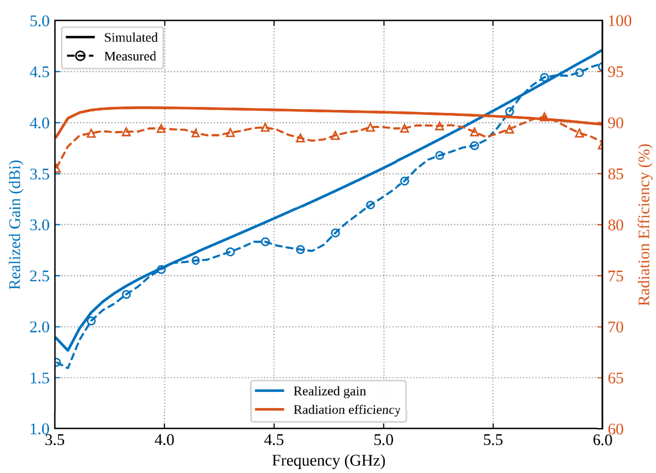

FIGURE 11. Simulated and measured realized gains and radiation efficiencies of the proposed antenna across the operating band.

only modal resistances R_i and shunt C_g are fitted — so resonant frequencies come from geometry rather than from optimisation. The input reflection follows from the input impedance at the port,

$$S_{11} = \frac{Z_{\text{in}} - Z_0}{Z_{\text{in}} + Z_0} \tag{6}$$

Table 2 lists the extracted values. The fitted branch resonances of 3.66, 4.87, and 6.10 GHz sit within 1.7% of closed-form values 3.72, 4.84, and 6.02 GHz, and the small offsets reflecting coupling between rings through the spokes that the isolated-ring equation does not include. Fig. 13 compares the circuit reflection with the full-wave response. The two agree with an RMS error of 0.72 dB across the band; the two resonance depths and the mid-band level are reproduced, and the only notable deviation is near the 3.5 GHz edge where the full-wave curve grazes -10 dB. The slope impedance is weakly constrained by a single-port magnitude fit above about 300 Ω and is therefore fixed rather than optimised, which keeps every branch value physical while preserving the fit.

Explicit inter-ring coupling elements are not included because cross-spokes inherently couple ring currents, while rings share a common radiator node and ground. Hence, the dominant inter-ring coupling is already represented by the shared node quantities of the parallel-branch topology, avoiding redundant circuit elements. Because the rings resonate in separated sub-bands, their modal overlap is weak, and the residual coupling is a second-order effect — its magnitude is precisely the $\leq 1.7\%$ offset between fitted and closed-form branch resonances, which is absorbed into fitted resistances and small resonance shifts. Finally, mutual-coupling parameters are not uniquely identifiable from a single-port magnitude fit; adding

TABLE 3. Comparison with recent sub-6 GHz ring, monopole, and CMA-based antennas.

Ref.	Year	Substrate (ε_r)	Band (GHz)	FBW	Ports	CMA-designed	Continuous single-port sub-6
[4]	2024	Rogers (2.2)†	3.2–7.3	78%	1/MIMO	No	Yes
[7]	2024	FR-4 (4.4)	5.73–10.78	61%	1	Yes	No (UWB, not sub-6)
[8]	2024	FR-4 (4.4)	3.4–3.8†	∼11%	4	Yes	No
[11]	2024	Rogers (3.5)†	3.55–3.80; 4.60–4.80	dual	4	No	No
[12]	2025	FR-4 (4.4)	3.30–3.78; 4.30–5.15	dual	2	No	No
[13]	2026	FR-4 (4.4)	n77/n78†	wideband	4	No	No
[15]	2022	FR-4 (4.4)†	3.2–6.0	61%	8	No	Yes (6-dB BW)
This work	—	RT/Duroid 5880 (2.2)	3.50–6.15	54.9%	1	Yes	Yes

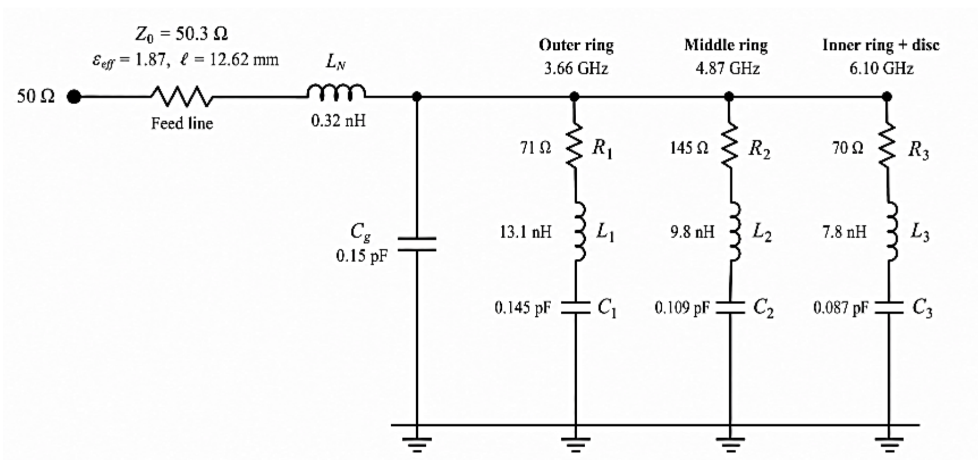

FIGURE 12. Physically partitioned equivalent circuit of the proposed antenna, one series-RLC branch per concentric ring.

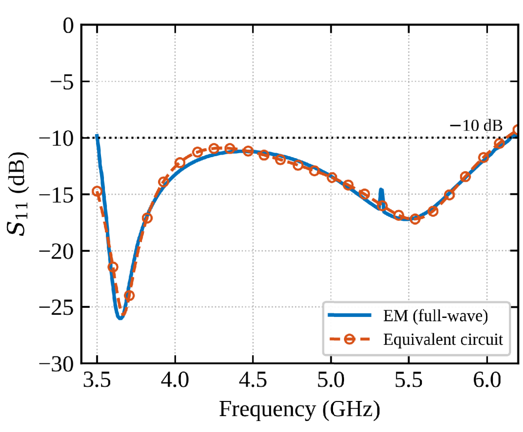

FIGURE 13. Full-wave (EM) and equivalent-circuit reflection coefficient of the proposed antenna.

them would reduce the physical meaning of each branch without improving the 0.72 dB RMS agreement.

9. COMPARISON WITH RECENT WORK

Table 3 compares the proposed antenna with recent ring, monopole, and CMA-based designs. The comparison is drawn on the axes where the design genuinely leads: it uses the lowest-permittivity substrate in the set, keeps a compact single-port footprint, and covers the full sub-6 band in one continuous match with a CMA-driven, ring-per-mode design chain. Several compared works reach a wider fractional bandwidth, but they begin nearer 3.1–3.2 GHz, and a lower starting frequency inflates the fractional bandwidth rather than indicating a wider match; several also rely on FR-4, where the higher permittivity assists miniaturisation. The proposed antenna trades a slightly narrower fractional bandwidth for a low-permittivity substrate and a fully continuous single-port band tied to a modal design method.

In short, no design in Table 3 combines all of the following: the lowest substrate permittivity in the set, a single feed port, a continuous rather than multi-resonance match across the full sub-6 band, and a CMA-driven ring-per-mode design chain backed by closed-form resonance equations. It is this combination, rather than raw fractional bandwidth, that constitutes the advance; the wider fractional bandwidths reported elsewhere largely reflect a lower start frequency, which inflates the percentage without indicating a wider match.

10. CONCLUSION

This paper designs a concentric multi-ring circular monopole by treating each ring as a separate characteristic-mode resonator and merging ring resonances into one continuous sub-6 GHz band. Characteristic mode analysis placed and ordered the ring modes before applying the feed, and closed-form ring-resonance equations predicted the band edges within 1.9% of measurement. Cross spokes maintain in-phase ring currents, while the triangular tapered partial ground, approximately one-quarter wavelength at the band center, completes the impedance matching. The antenna occupies $0.27\lambda_0 \times 0.39\lambda_0$ on RT/Duroid 5880 and covers 3.50–6.15 GHz, a 54.9% band spanning the n77, n78 and n79 5G NR bands and the 5.5 GHz WLAN band from a single port. A physically partitioned equivalent circuit, one series-RLC branch per ring with each branch resonance fixed to its closed-form value, reproduced the full-wave reflection response to 0.72 dB RMS. The result is a compact, single-layer, single-feed antenna for continuous sub-6 GHz coverage whose every dimension is tied to a resonant mechanism.

The present study concerns a single-element radiator, and the metrics reported here — impedance bandwidth, gain, efficiency, and radiation patterns — are the appropriate figures of merit. Diversity metrics, such as ECC, channel-capacity loss, and specific-absorption-rate evaluation, apply to multi-element or on-body deployments and are therefore outside the present single-port, non-wearable scope; a multi-element MIMO arrangement of the proposed element, using decoupling techniques discussed in Section 2, is a natural direction for future work.

REFERENCES

[1] Harrington, R. and J. Mautz, "Theory of characteristic modes for conducting bodies," *IEEE Transactions on Antennas and Propagation*, Vol. 19, No. 5, 622–628, September 1971.

[2] Garbacz, R. and R. Turpin, "A generalized expansion for radiated and scattered fields," *IEEE Transactions on Antennas and Propagation*, Vol. 19, No. 3, 348–358, May 1971.

[3] Adams, J. J. and J. T. Bernhard, "Broadband equivalent circuit models for antenna impedances and fields using characteristic modes," *IEEE Transactions on Antennas and Propagation*, Vol. 61, No. 8, 3985–3994, August 2013.

[4] Iriqat, S., S. Yenikaya, and M. Secmen, "Design and characterization of a circular ring monopole antenna and its MIMO configuration for sub-6 GHz, sub-7 GHz and mm-Wave 5G applications," *Physica Scripta*, Vol. 99, No. 12, 125533, 2024.

[5] Han, M. and W. Dou, "Compact clock-shaped broadband circularly polarized antenna based on characteristic mode analysis," *IEEE Access*, Vol. 7, 159 952–159 959, 2019.

[6] Tran, H. H., N. Nguyen-Trong, and A. M. Abbosh, "Simple design procedure of a broadband circularly polarized slot monopole antenna assisted by characteristic mode analysis," *IEEE Access*, Vol. 6, 78 386–78 393, 2018.

[7] Heo, H., M.-J. Kang, S. Park, J. Lee, L. Qu, and K.-Y. Jung, "Design of a UWB circularly-polarized planar monopole antenna using characteristic mode analysis," *Scientific Reports*, Vol. 14, No. 1, 26236, 2024.

[8] Khan, R., W. T. Sethi, W. A. Malik, L. Jan, M. M. Tahseen, A. M. Almuhlafi, and M. Himdi, "Enhancing gain and isolation of a quad-element MIMO antenna array design for 5G sub-6 GHz applications assisted with characteristic mode analysis," *Scientific Reports*, Vol. 14, No. 1, 11111, 2024.

[9] Fazal, D., Q. U. Khan, and I.-P. Hong, "Multiband antenna design with enhanced radiations using characteristic mode analysis," *Scientific Reports*, Vol. 13, No. 1, 17829, 2023.

[10] Ullah, U., S. Koziel, and A. Pietrenko-Dabrowsks, "Characteristics mode analysis and excitation of orthogonal modes on a single substrate for wideband IoT applications in the millimeter wave band," *Scientific Reports*, Vol. 15, No. 1, 8810, 2025.

[11] Chakraborty, S., M. A. Rahman, M. A. Hossain, E. Nishiyama, and I. Toyoda, "A novel dual-band elliptical ring slot MIMO antenna with orthogonal circular polarization for 5G applications," *Heliyon*, Vol. 10, No. 13, e33176, 2024.

[12] Chand, N. G. and K. Anusudha, "Compact two-port dual- and triple-band MIMO antennas with orthogonally placed microstrip monopole elements for 5G N77/78/79 sub-6-GHz applications," *International Journal of Communication Systems*, Vol. 38, No. 13, e70183, 2025.

[13] Kanisha, R. K., C. Rimmya, and M. G. Madhan, "Compact quad-port dual-polarized wideband MIMO antenna with rotational-symmetry decoupling element for n77/n78 band diversity," *International Journal of Communication Systems*, Vol. 39, No. 4, e70430, 2026.

[14] Dhananjeyan, R., S. Ramesh, D. R. Kumar, and O. P. Kumar, "Compact octagonal MIMO antenna system for broadband applications with enhanced isolation and wideband performance," *Scientific Reports*, Vol. 15, No. 1, 18921, 2025.

[15] Jiang, J.-Y. and H.-L. Su, "A wideband eight-element MIMO antenna array in 5G NR n77/78/79 and WLAN-5 GHz bands for 5G smartphone applications," *International Journal of Antennas and Propagation*, Vol. 2022, No. 1, 8456936, 2022.

[16] Moradikordalivand, A., T. A. Rahman, S. Ebrahimi, and S. Hakimi, "An equivalent circuit model for broadband modified rectangular microstrip-fed monopole antenna," *Wireless Personal Communications*, Vol. 77, No. 2, 1363–1375, 2014.

[17] Liang, J., C. C. Chiau, X. Chen, and C. G. Parini, "Printed circular ring monopole antennas," *Microwave and Optical Technology Letters*, Vol. 45, No. 5, 372–375, June 2005.

[18] Sandeep, D. R., A. H. M. Almawgani, S. Salma, K. S. Kumar, A. R. H. Alhawari, P. V. Santhi, and B. T. P. Madhav, "Smart antenna with conductive fabric for internet of things applications: A fusion of comfort and connectivity," *The European Physical Journal Plus*, Vol. 141, No. 3, 246, March 2026.

[19] Bait-Suwailam, M. M., O. F. Siddiqui, and O. M. Ramahi, "Mutual coupling reduction between microstrip patch antennas using slotted-complementary split-ring resonators," *IEEE Antennas and Wireless Propagation Letters*, Vol. 9, 876–878, 2010.

[20] Alhaqbani, H. S., M. M. Bait-Suwailam, M. A. Aldhaeebi, and T. S. Almoneef, "Wideband diversity MIMO antenna design with hexagonal slots for 5G smart mobile terminals," *Progress In Electromagnetics Research C*, Vol. 120, 105–117, 2022.

[21] Ghawbar, F., J. A. Sukur, H. A. Majid, M. M. Bait-Suwailam, H. Al-Lawati, A. A. G. Amer, F. A. Saparudin, and A. S. A. Ghafar, "Highly self-isolated 12-MIMO antenna elements for 5G mobile applications," *Electronics*, Vol. 14, No. 7, 1424, 2025.